Supplementary Information

Invigorating the Catalytic Activity of Cobalt Selenide via Structural Phase Transition Engineering for Lithium-Oxygen Battery

Minglu Li[a], Chaozhu Shu*[a], Anjun Hu[b], Jiabao Li[a], Ranxi Liang[a], Jianping Long*[a]

[a]College of Materials and Chemistry & Chemical Engineering, Chengdu University of Technology, 1#, Dongsanlu, Erxianqiao, Chengdu 610059, Sichuan, P. R. China

[b]State Key Laboratory of Electronic Thin Films and Integrated Devices, University of Electronic Science and Technology of China, Chengdu, 610054, Sichuan, P. R. China

*Corresponding author:

Email: czshu@imr.ac.cn (Chaozhu Shu); longjianping@cdut.cn (Jianping Long)

The number of pages: 14 (S1-S14)

The number of Figures: 15 (Figures S1-S15)

The number of Tables: 4 (Tables S1-S4)

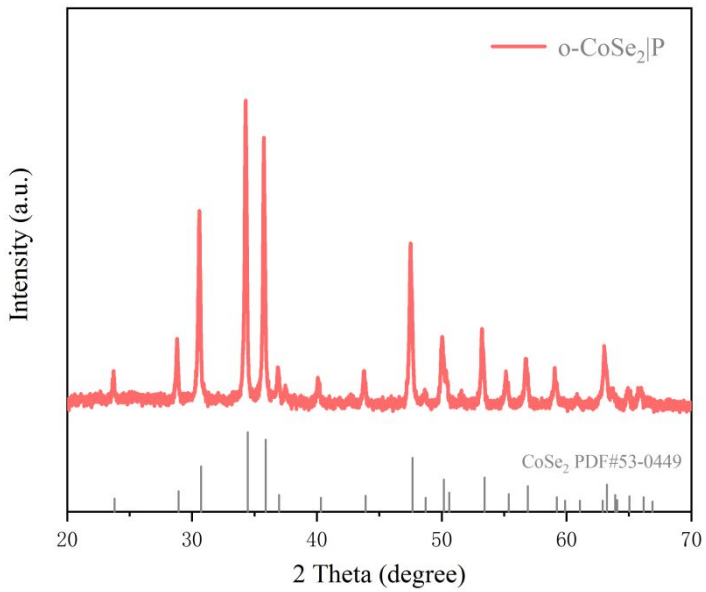

Figure S1 XRD patterns of the o-$CoSe_2$|P.

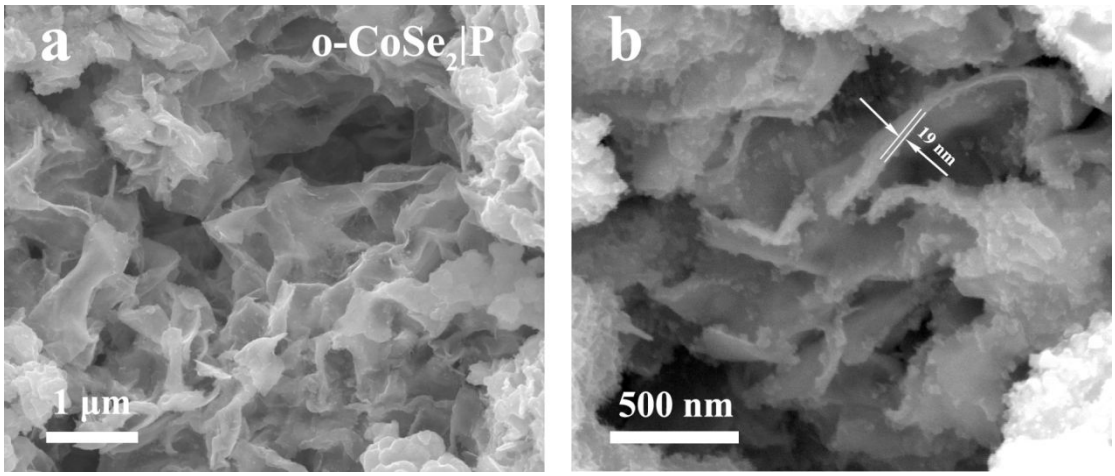

Figure S2 a) and b) SEM image of o-$CoSe_2$|P nanobelts. o-$CoSe_2$|P maintains an excellent nanobelt structure with a thickness of about 19 nm.

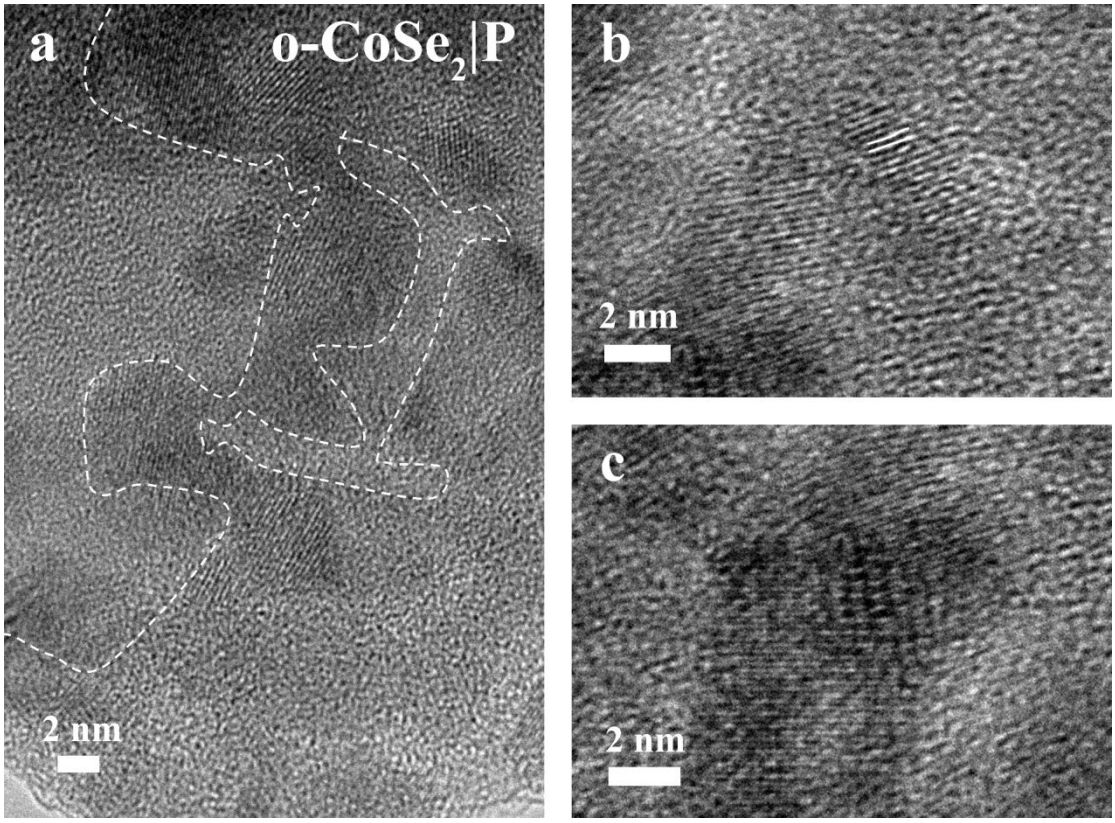

Figure S3 a)-c) High-resolution TEM (HRTEM) images of o-$CoSe_2$|P. HRTEM image of o-$CoSe_2$|P shows defects around the edge of the hole. These defects are caused by heat treatment and bond rotation during the phase change, which creates more active sites and is beneficial for OER catalysis.

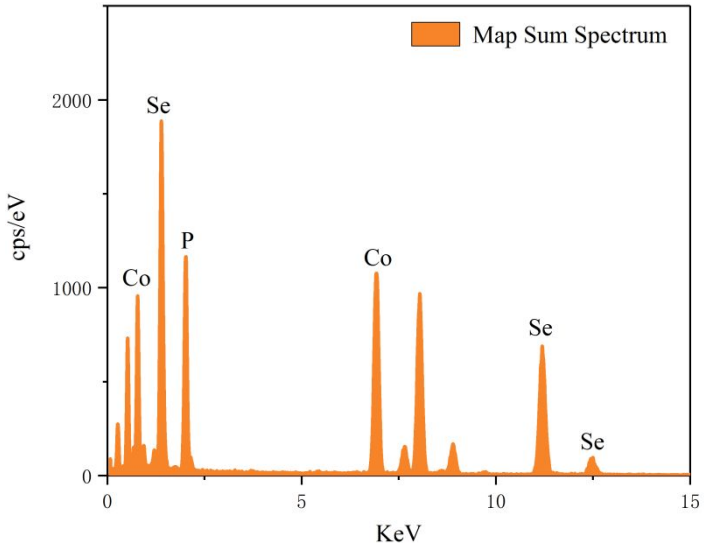

Figure S4 EDX pattern of o-$CoSe_2$|P.

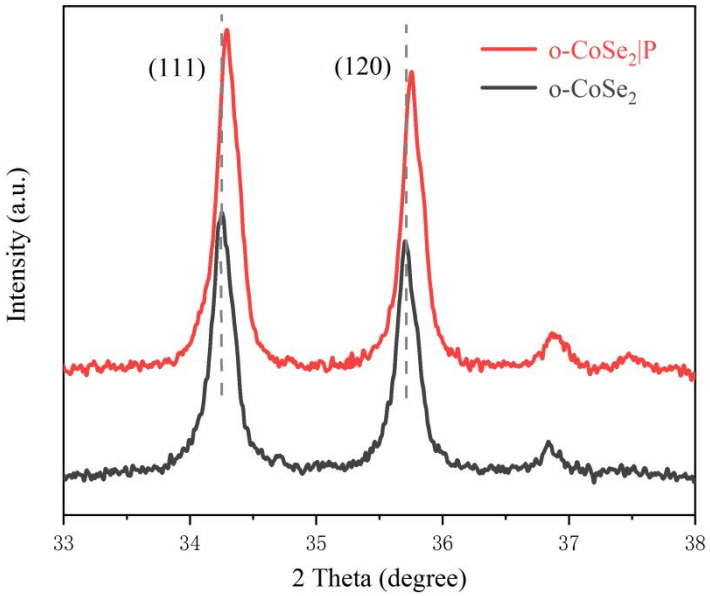

Figure S5 XRD pattern of orthogonal phase o-$CoSe_2$ without P doping and o-$CoSe_2$|P (JCPDS: 53-0449).

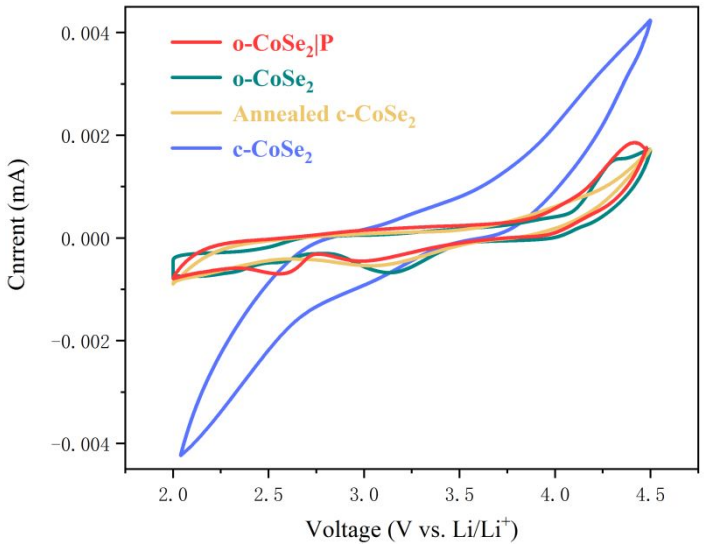

Figure S6 CV curves of the Li-O_2 batteries based on o-$CoSe_2$|P, o-$CoSe_2$, annealed c-$CoSe_2$ and c-$CoSe_2$ electrodes.

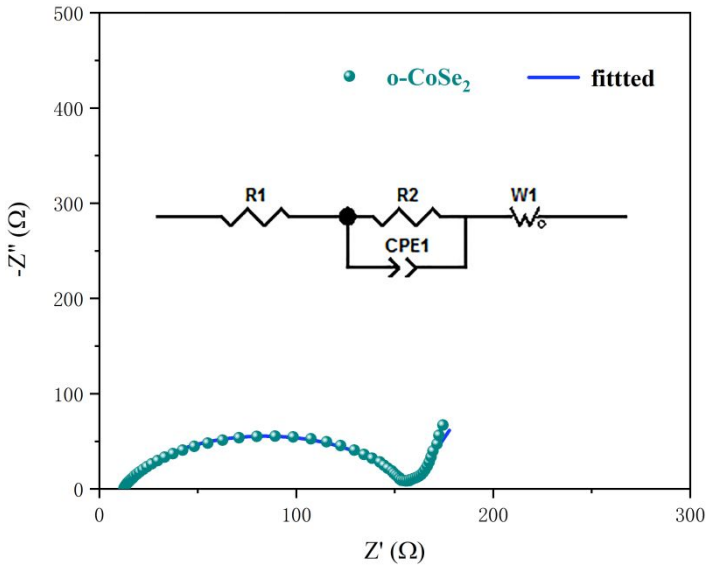

Figure S7 Nyquist plots of Li-O_2 batteries based on o-$CoSe_2$ electrodes.

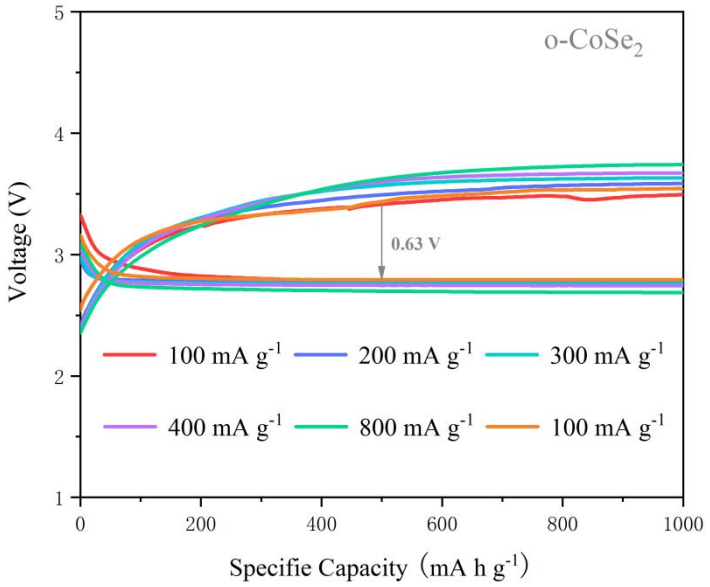

Figure S8 Rate capability of Li-O_2 batteries with annealed o-$CoSe_2$.

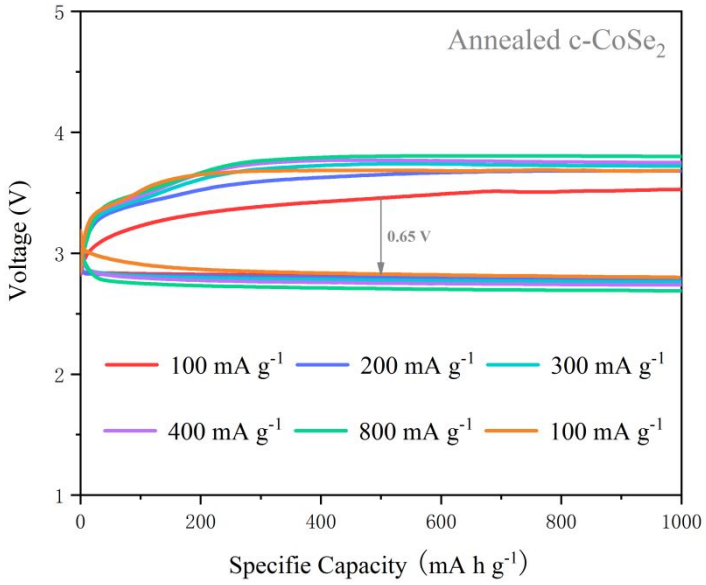

Figure S9 Rate capability of Li-O_2 battery with annealed c-$CoSe_2$.

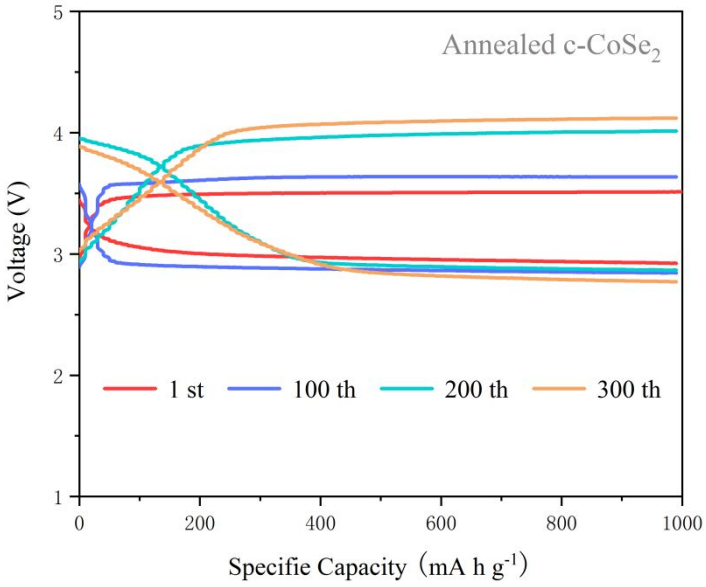

Figure S10 Discharge and charge curves of Li-O_2 batteries with annealed c-$CoSe_2$.

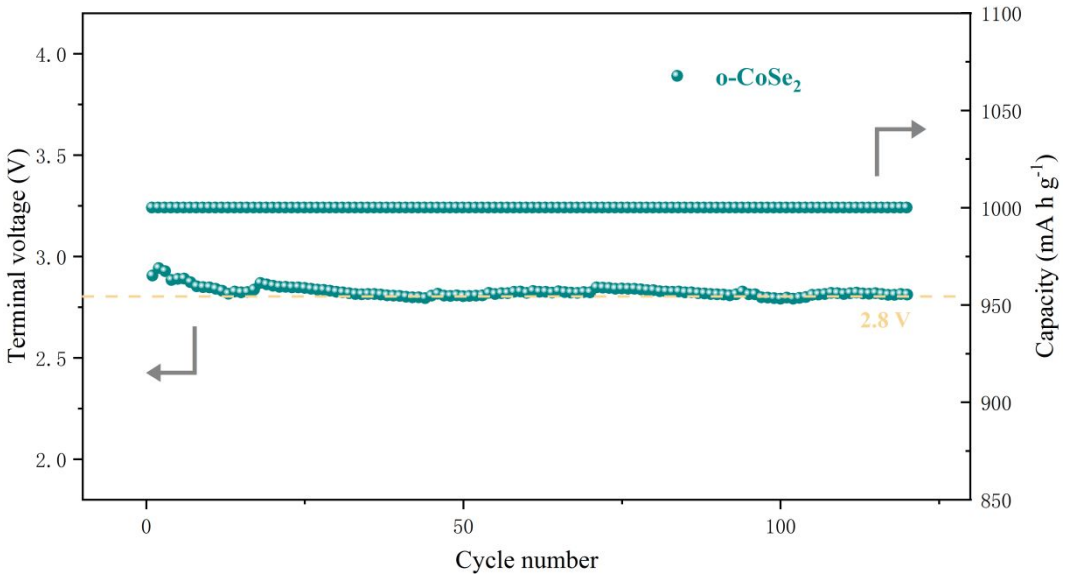

Figure S11 Cycling performance of Li-O_2 batteries with o-$CoSe_2$ with a limited capacity of 1000 mA h g^{-1} at a current density of 50 mA g^{-1}.

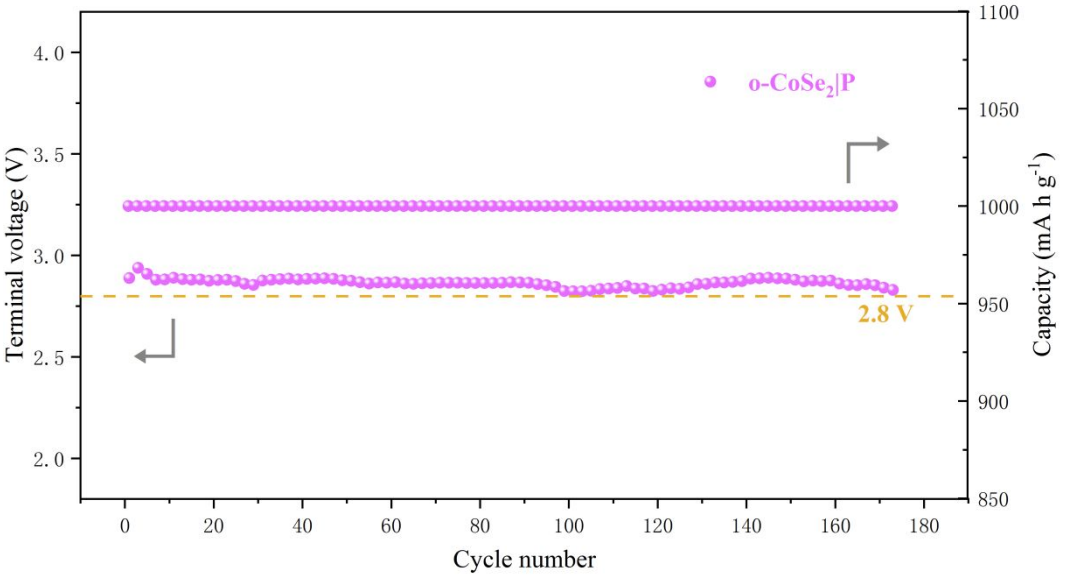

Figure S12 Cycling performance of Li-O_2 battery based on o-$CoSe_2$|P electrode at a current density of 200 mA g^{-1} with a limited specific capacity of 1000 mA h g^{-1}.

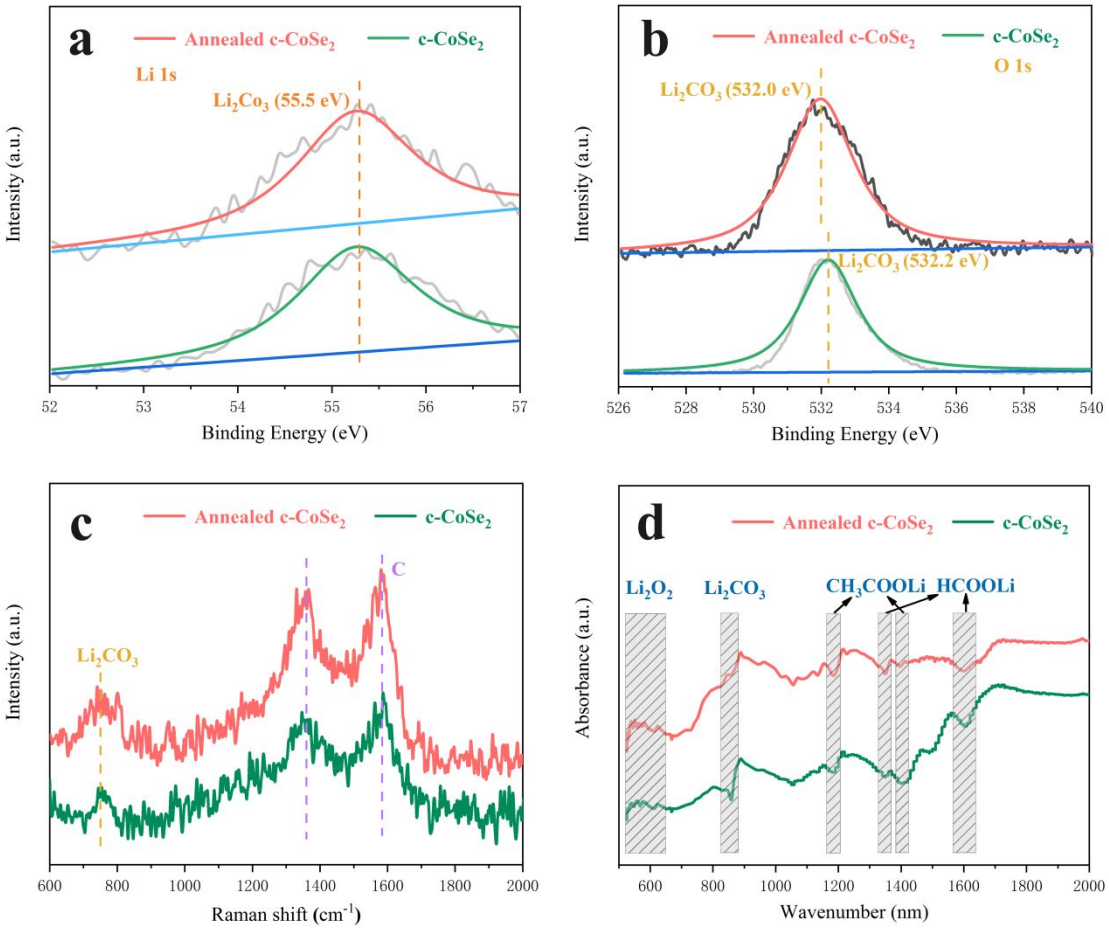

Figure S13 a) Li 1s XPS spectra, b) O 1s XPS spectra, c) Raman spectra and d) FTIR spectra of annealed c-$CoSe_2$ and c-$CoSe_2$ after 100 cycles.

As shown in Fig S13a, the Li 1S XPS spectra of the c-$CoSe_2$ and annealed c-$CoSe_2$ oxygen electrodes show peaks at about 55.5eV and 56.3eV after 100 cycles, which can be assigned to the discharged by-product Li_2CO_3 after cycling. In the O 1S XPS (Fig S13b), the characteristic peaks of c-$CoSe_2$ and annealed c-$CoSe_2$ oxygen electrode after 100 cycles at about 532.0 eV can be attributed to discharge by-product Li_2CO_3. For the Raman spectra shown in Fig S11c, the c-$CoSe_2$ and annealed c-$CoSe_2$ oxygen electrodes show the characterization peak at about 749 cm^{-1} after 100 cycles, corresponding to the harmful by-products Li_2CO_3 generated after cycling. The peaks at 1352 cm^{-1} and 1580 cm^{-1} can be attributed to the carbon cloth substrate.

In order to better understand the discharged by-products on the electrode surface after cycling, Fourier transform infrared spectrum (FTIR) characterization on c-$CoSe_2$ and annealed c-$CoSe_2$ oxygen electrodes after 100 cycles was further carried out. The

different peaks around 400~600 cm^{-1} in the FTIR spectra shown in Fig S13d are due to the reversible formation and decomposition of Li_2O_2 on the surface of the c-$CoSe_2$ and annealed c-$CoSe_2$ oxygen electrodes. However, a characteristic absorption peak at 870 cm^{-1} was found in both electrodes and could be assigned to Li_2CO_3[S10]. The main reason for the formation of Li_2CO_3 is the oxidation of carbon substrate during the charging process. Moreover, Li_2CO_3 and other organic lithium salts (CH_3COOLi, HCOOLi) (1190 cm^{-1} and 1400 cm^{-1}, 1350 cm^{-1} and 1600 cm^{-1}) will cover the effective surface area for the formation and decomposition of Li_2O_2[S1]. In addition, as the cycle progresses, Li_2CO_3 and organolithium salts will gradually deposit on the oxygen electrode because these lithium salts are difficult to decomposition during charging. Finally, the active surface area will be totally covered and the passivation of the electrode surface will take place, leading to the death of the of c-$CoSe_2$ and annealed c-$CoSe_2$ electrodes[S2]

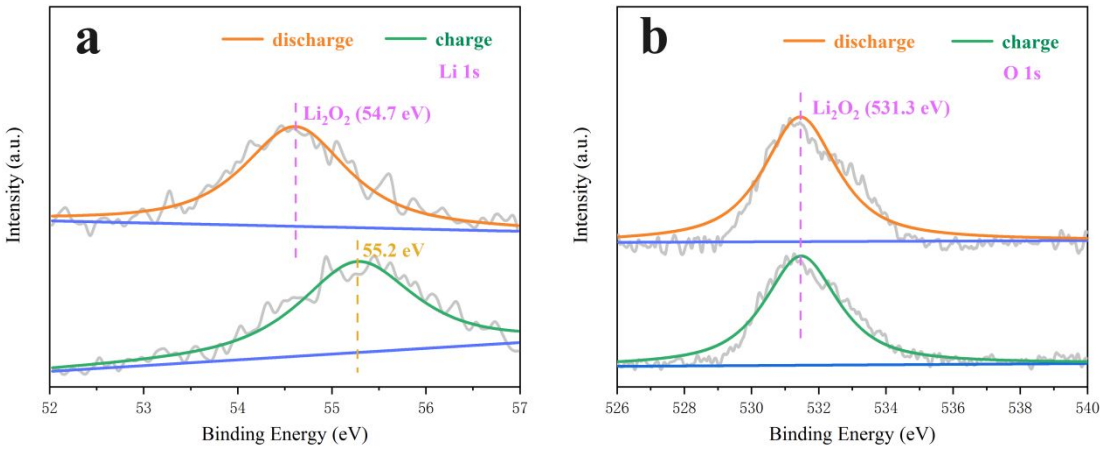

Figure S14 a) Li 1s XPS spectra and b) Li 1s XPS spectra of o-$CoSe_2$|P after discharge and after charge.

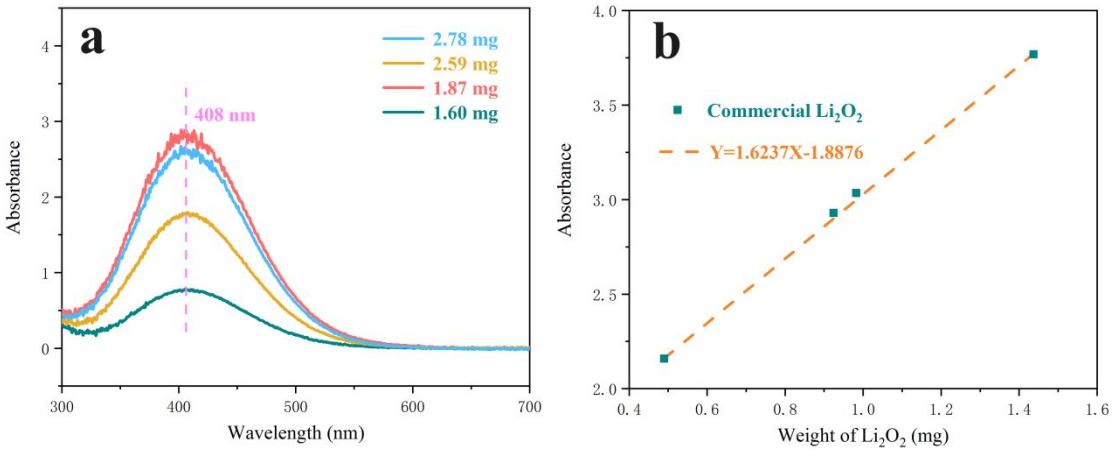

Figure S15 a) UV-Vis spectra of $TiOSO_4$ titration solution with different amount of commercial Li_2O_2. b) The fitted line and the corresponding linear equation.

Table S1. Corresponding element ratio of o-$CoSe_2$|P.

Element	Wt%
P	18.34
Co	35.67
Se	45.99

Table S2. Impedance parameters of the Li-O_2 battery after fitting raw data to an equivalent circuit.

Catalyst	R1	R2
o-$CoSe_2$|P	13.3	118.3
o-$CoSe_2$	13.5	136.5
Annealed c-$CoSe_2$	12	138
c-$CoSe_2$	60.62	178.9

Table S3. The amount of Li_2O_2 on the oxygen electrode at different discharge capacity.

Discharge capacity (mA h)	Calculated Li_2O_2 weight (mg)	Titrated weight of Li_2O_2 (mg)	Yield (%)
2.5	2.14	1.60	74.77
3	3.57	1.87	72.83
3.5	3.00	2.59	86.45
4	3.42	2.78	81.20

Table S4. Performance comparison of Li-O_2 batteries based on different oxygen electrodes.

Sample	Current density	Cut-off voltage (V)	Limited capacity (mA h g^{-1})	Number of cycles	Ref.
o-$CoSe_2$|P	50 mA g^{-1}	2	1000	500	This work
δ-MnO_2 nanoboxes	0.08 mA cm^{-2}	2	1000	113	S3
δ-MnO_2 /G	0.333 mA cm^{-2}	2.0	492	132	S4
ε-MnO_2	500 mA g^{-1}	2.2	800	190	S5
3D hollow α-MnO_2	200 mA g^{-1}	2.2	1000	170	S6
Co–Mn–O nanocube	0.16 mA cm^{-2}	>2.0	500	100	S7
Co@PNCS	250 mA g^{-1}	2.3	600	120	S8

Co_3O_4/GN	300 mA g^{-1}	≈2.7	1500	42	S9
CuCr2O4@rGO	200 mA g^{-1}	2	1000	100	S10
Co_3O_4-TiO_2(B)	100 mA g^{-1}	≈2.6	1000	200	S11
Co@N-C microspheres	0.1 mA cm^{-2}	2.2	500	40	S12
nitrogen-doped $LaNiO_3$	250 mA g^{-1}	2.6	500	50	S13
NiO	0.1 mA cm^{-2}	2.3	800	50	S14
$CoSe_2$ @G-C_3N_4	0.3 mA cm^{-2}	2	<1000	30	S15
3D M-MoSSe	50 mA g^{-1}	2.4	<1000	30	S16
5%Pt+5%Cu	100 mA g^{-1}	2.2	500	50	S17

Note: G=graphene, PNCS=N-porous doped carbon nanosheets, GN=graphene nanosheets.

By comparing the performance of Li-O_2 batteries based on different oxygen electrodes, it can be found that the o-$CoSe_2$|P based Li-O_2 battery proposed in this work demonstrates much better cycle stability as compared to previous reported metal oxides such as MnO_2, Co_3O_4, NiO and metal selenides such as $CoSe_2$, $MoSe_2$. Thus,

comparing with previous reported oxygen electrodes, the o-$CoSe_2$|P oxygen electrode demonstrates much obvious competitiveness, thus providing a new strategy for developing efficient oxygen electrode for Li-O_2 battery. We have added the above discussion to the supporting information (Table S4).

Reference

(S1) Zhang, P.; Zhang, S.; He, M.; Lang, J.; Ren, A.; Xu, S.; Yan, X. Realizing the Embedded Growth of Large Li_2O_2 Aggregations by Matching Different Metal Oxides for High–Capacity and High–Rate Lithium Oxygen Batteries. *Adv. Sci.* **2017,** *4*, 1700172, DOI 10.1002/advs.201700172.

(S2) Wang, P.; Li, C.; Dong, S.; Ge, X.; Zhang, P.; Miao, X.; Wang, R.; Zhang, Z.; Yin, L. Hierarchical $NiCo_2S_4$@NiO Core–Shell Heterostructures as Catalytic Cathode for Long–Life Li–O_2 Batteries. *Adv. Energy Mater.* **2019**, *9,* 1900788, DOI 10.1002/aenm.201900788.

(S3) Zhang, J.; Luan, Y.; Lyu, Z.; Wang, L.; Xu, L.; Yuan, K.; Pan, F.; Lai, M.; Liu, Z.; Chen, W. Synthesis of Hierarchical porous δ–MnO_2 Nanoboxes as an Efficient Catalyst for Rechargeable Li-O_2 Batteries. *Nanoscale* **2015,** *7*, 14881–14888, DOI 10.1039/C5NR02983J.

(S4) Liu, S.; Zhu, Y.; Xie, J.; Huo, Y.; Yang, H. Y.; Zhu, T.; Cao, G.; Zhao, X.; Zhang, S. Direct Growth of Flower–Like δ–MnO_2 on Three–Dimensional Graphene for High-Performance Rechargeable Li-O_2 Batteries. *Adv. Energy Mater.* **2014,** *4*, 1301960, DOI 10.1002/aenm.201301960.

(S5) Hu, X.; Cheng, F.; Han, X.; Zhang, T.; Chen, J. Oxygen Bubble-Templated Hierarchical Porous ε-MnO_2 as a Superior Catalyst for Rechargeable Li–O_2 Batteries. *Small* **2015,** *11*, 809–813, DOI 10.1002/smll.201401790.

(S6) Bi, R.; Liu, G.; Zeng, C.; Wang, X.; Zhang, L.; Qiao, S. Z. 3D Hollow α–MnO2 Framework as an Efficient Electrocatalyst for Lithium–Oxygen Batteries. *Small* **2019,** *15*, 1804958, DOI 10.1002/smll.201804958.

(S7) Zhang, J.; Wang, L.; Xu, L.; Ge, X.; Zhao, X.; Lai, M.; Liu, Z.; Chen, W. Porous Cobalt–Manganese Oxide Nanocubes Derived from Metal Organic Frameworks as a Cathode Catalyst for Rechargeable Li–O_2 Batteries. *Nanoscale* **2015,** *7*, 720–726, DOI 10.1039/C4NR05865H.

(S8) Zhai, Y.; Wang, J.; Gao, Q.; Fan, Y.; Hou, C.; Hou, Y.; Liu, H.; Shao, Q.; Wu, S.; Zhao, L. Highly Efficient Cobalt Nanoparticles Anchored Porous N-doped Carbon Nanosheets Electrocatalysts for Li–O_2 Batteries. *J. Catal.* **2019,** *377*, 534–542, DOI 10.1016/j.jcat.2019.07.055.

(S9) Yuan, M.; Yang, Y.; Nan, C.; Sun, G.; Li, H.; Ma, S. Porous Co_3O_4 Nanorods Anchored on Graphene Nanosheets as an Effective Electrocatalysts for Aprotic Li–O_2 Batteries. *Appl. Surf. Sci.* **2018,** *444*, 312–319, DOI 10.1016/j.apsusc.2018.02.267.

(S10) Liu, J.; Zhao, Y.; Li, X.; Wang, C.; Zeng, Y.; Yue, G.; Chen, Q. $CuCr_2O_4$@rGO Nanocomposites as High-Performance Cathode Catalyst for Rechargeable Lithium-Oxygen Batteries. *Nano–Micro Lett.* **2018,** *10*, 22, DOI 10.1007/s40820-017-0175-z.

(S11) Wang, G.; Zhang, S.; Qian, R.; Wen, Z. Atomic–Thick TiO_2 (B) Nanosheets Decorated with Ultrafine Co_3O_4 Nanocrystals As a Highly Efficient Catalyst for Lithium–Oxygen Battery. *ACS Appl. Mater. Interfaces* **2018,** *10*, 41398–41406, DOI 10.1021/acsami.8b15774.
(S12) Song, J.; Lv, X.; Jiao, Y.; Wang, P.; Xu, M.; Li, T.; Chen, X.; Li, J.; Zhang, Z. Catalyst Nanoarchitecturing via Functionally Implanted Cobalt Nanoparticles in Nitrogen Doped Carbon Host for Aprotic Lithium–Oxygen Batteries. *J. Power Sources* **2018,** *394*, 122–130, DOI 10.1016/j.jpowsour.2018.05.058.
(S13) Zhang, J.; Zhang, C.; Li, W.; Guo, Q.; Gao, H.; You, Y.; Li, Y.; Cui, Z.; Jiang, K.-C.; Long, H. Nitrogen–Doped Perovskite as a Bifunctional Cathode Catalyst for Rechargeable Lithium–Oxygen Batteries. *ACS Appl. Mater. Interfaces* **2018,** *10*, 5543–5550, DOI 10.1021/acsami.7b17289.
(S14) Dong, H.; Tang, P.; Zhang, S.; Xiao, X.; Jin, C.; Gao, Y.; Yin, Y.; Li, B.; Yang, S. Excellent oxygen evolution reaction of NiO with a layered nanosphere structure as the cathode of lithium–oxygen batteries. *RSC Adv.* **2018,** *8*, 3357–3363, DOI 10.1039/C7RA12630A.
(S15) Kumar, S.; Jena, A.; Hu, Y. C.; Liang, C.; Zhou, W.; Hung, T. F.; Chang, W. S.; Chang, H.; Liu, R. S. Cobalt Diselenide Nanorods Grafted on Graphitic Carbon Nitride: A Synergistic Catalyst for Oxygen Reactions in Rechargeable Li–O_2 Batteries. *ChemElectroChem* **2018,** *5*, 29–35, DOI 10.1002/celc.201700909.
(S16) Zhang, S.; Huang, Z.; Wen, Z.; Zhang, L.; Jin, J.; Shahbazian-Yassar, R.; Yang, J. Local lattice distortion activate metastable metal sulfide as catalyst with stable full discharge–charge capability for Li–O_2 batteries. *Nano Lett.* **2017,** *17*, 3518–3526, DOI 10.1021/acs.nanolett.7b00603.
(S17) Luo, X.; Ge, L.; Ma, L.; Kropf, A. J.; Wen, J.; Zuo, X.; Ren, Y.; Wu, T.; Lu, J.; Amine, K. Effect of Componential Proportion in Bimetallic Electrocatalysts on the Aprotic Lithium–Oxygen Battery Performance. *Adv. Energy Mater.* **2018,** *8*, 1703230, DOI 10.1002/aenm.201703230.